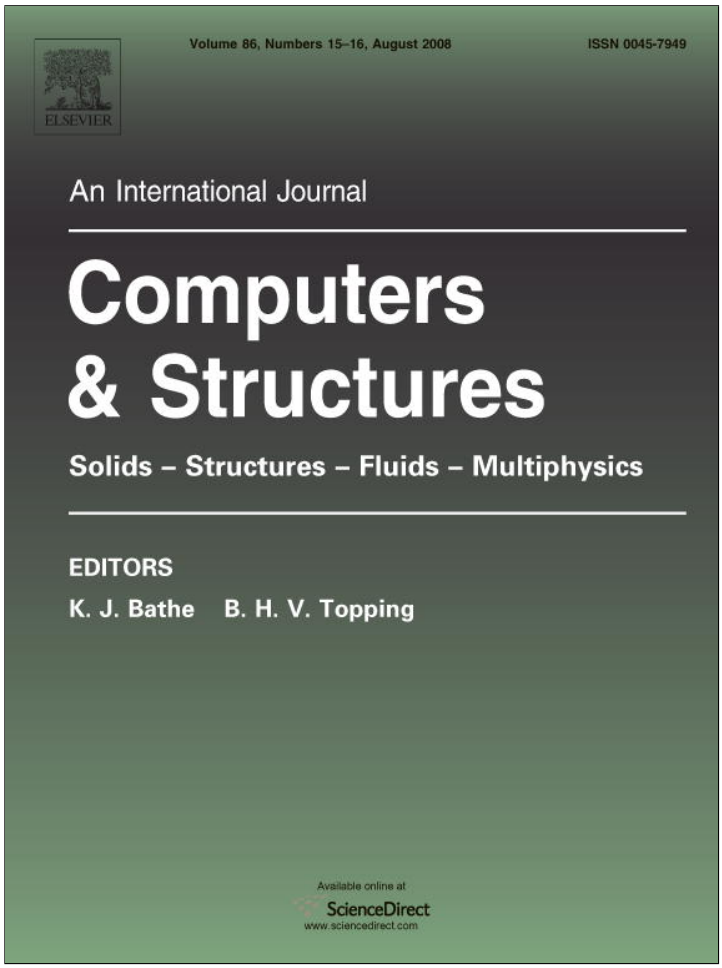

Available online at www.sciencedirect.com
ScienceDirect
Computers and Structures 86 (2008) 1604–1618
Computers & Structures
www.elsevier.com/locate/compstruc

A numerical procedure simulating RC structures reinforced with FRP using the serial/parallel mixing theory

Xavier Martinez *, Sergio Oller, Fernando Rastellini, Alex H. Barbat

Departament de Resistència de Materials i Estructures a l'Enginyeria (RMEE), Universitat Politècnica de Catalunya (UPC), Jordi Girona 1-3, Mòdul C1, Campus Nord, 08034 Barcelona, Spain

Received 20 February 2007; accepted 17 January 2008
Available online 5 March 2008

Abstract

The use of fiber reinforced polymers (FRP) to reinforce and retrofit reinforced concrete (RC) structures has become one of the main applications of composites in civil engineering. This paper describes a procedure, based on a finite element formulation, that can be used to perform numerical simulations of RC structures reinforced with FRP. Composites are treated using the serial/parallel mixing theory, which deduces the composite behavior from the constitutive equations of its components. A new construction-stages algorithm is developed for simulating retrofitted structures. The performance of the proposed formulation is proved comparing numerical and experimental results. Finally, the developed code is used to obtain the optimum FRP reinforcement configuration for a RC frame structure.

Keywords: RC structures; FRP reinforcement; Retrofitting; Composite materials; Serial/parallel mixing theory

1. Introduction

The first known report in which carbon fiber reinforced polymers (CFRP) were used to retrofit a damaged structure is from 1991, when they were used to strengthen the Ibach Bridge in Lucerne, Switzerland [1]. Since then, this technology has become far more widely used and is now one of the main applications of composite materials in civil engineering.

Most current knowledge about the structural reinforcement and/or retrofitting of reinforced concrete (RC) structures with fiber reinforced polymers (FRP) is based on experimental simulations, that are used to analyze different reinforcement applications such as bending reinforcements [2], shear reinforcements [3,4], column wrapping [5] or anchorage of the reinforcement to the existing structure [6]. These studies use experimental techniques that are supported and complemented by analytical calculations. If the problem is treated numerically, material nonlinearities are usually linearized and the FRP composite is considered as a single material (i.e. [7]).

On the other hand, composite materials have been, and still are, one of the principal areas of research in computational mechanics throughout the last few decades. Main efforts are focused on the study of composite plates and shells [8,9], as these are the structural elements commonly used in aeronautical, nautical and automotive structures, which are the engineering fields in which composites are most widely applied.

Traditionally, numerical simulations of composites have been performed using orthotropic materials with average properties from their constituents. With this approach, no model has been found that is able to function beyond the elastic limit state of its constituents. As a result, numerical simulations are limited to elastic cases. Different theories have been proposed to solve this problem which take into account the internal configuration of the composite to predict its behavior. The two most commonly used are described below.

* Corresponding author. Tel.: +34 934016473; fax: +34 934011048.
E-mail addresses: xaviermg@cimne.upc.edu (X. Martinez), sergio.oller@upc.edu (S. Oller), frastel@cimne.upc.edu (F. Rastellini), alex.barbat@upc.edu (A.H. Barbat).

0045-7949/$ - see front matter © 2008 Elsevier Ltd. All rights reserved.
doi:10.1016/j.compstruc.2008.01.007

Homogenization theory: This method deals with the global composite structure problem in a two-scale context. On the macroscopic scale the composite materials determine the global response of the structure. Composites are considered to be homogeneous materials in this scale. The microscopic scale represents an elemental characteristic volume in which the microscopic fields inside the composite are obtained. This scale deals with the component materials of the composite, each one with its own constitutive equation. Homogenization theory relates these two scales by assuming a periodic configuration of the composite material [10,11].
Mixing theory: The first formulation of the mixing theory was developed by Truesdell and Toupin [12] and it is based on two main hypotheses: 1. All composite constituents are subject to same strains. 2. Each constituent contributes to the composite behavior according to its volumetric participation. The main drawback of the mixing theory is the iso-strain condition which enforces a parallel distribution of the constituents in the composite. Some improvements to the original formulation can be found in [13,14].

Despite all the existing studies on both subjects, experimental tests of FRP reinforcements and numerical characterization of composite materials, little research has used a numerical approach to analyze the structural reinforcement of RC structures with FRP. Therefore, the main goal of this paper is to combine both fields, developing a numerical procedure for computing RC structures reinforced with FRP. The developed formulation is based on the finite element method and enables determining the structural performance of existing structures when they are reinforced and/or retrofitted with FRP. This performance is calculated taking into account material nonlinearities. The developed formulation also identifies the performance of each constituent material in the structure (for example, it is possible knowing the stress state of the fiber in the composite reinforcement when the structure collapses). The code can be used to study the same structure with different FRP configurations, to determine the most suitable option for the case considered. It can also apply the reinforcement to structures that are already damaged, reproducing with more accuracy the conditions found in real applications.

The numerical formulations proposed in this paper use the serial/parallel rule of mixtures, developed by Rastellini [15], to analyze composite materials. The code also includes a construction-stages algorithm that is used to consider the case of structural retrofitting. Section 2 contains a detailed description of both of these features. In Section 3 the experimental data reported in [2] for a RC beam reinforced with CFRP is used to validate the proposed code. Two different numerical simulations are then described to illustrate the potential of the formulation developed: The first case, in Section 4, shows the results obtained when the RC beam used to validate the code is retrofitted. The second case, in Section 5, uses the code to simulate a concrete frame structure in which different FRP reinforcements are applied to the beam, column and beam–column connecting joint. This simulation illustrates how the developed code can be used to determine which FRP reinforcement configuration achieves better results. Finally, in Section 6, are presented the conclusions about the numerical tool developed and the conclusions drawn from the calculations performed.

2. Numerical formulation

2.1. Serial/parallel rule of mixtures

The serial/parallel rule of mixtures is an improvement of the classical mixing theory, in which the iso-strain hypothesis is replaced by an iso-strain condition in the fiber direction and an iso-stress condition in the transversal directions. This theory was developed by Rastellini and is explained in detail in [15].

2.1.1. Definition of the serial and parallel components of the strain and stress tensors

The serial/parallel (SP) model considers that the constituent materials of the composite act in parallel in a certain direction and in serial in the remaining directions. Consequently, it is necessary to define and separate the serial and parallel components of the strain and stress tensors.

Defining e_1 as the director vector that determines the parallel behavior (fiber direction), the parallel projector tensor N_P can be defined as follows:

$$N_P = e_1 \otimes e_1. \tag{1}$$

From N_P, the fourth-order parallel projector tensor, P_P, is defined as

$$P_P = N_P \otimes N_P. \tag{2}$$

The serial projector tensor P_S is evaluated as its complement:

$$P_S = I - N_P. \tag{3}$$

Both tensors can be used to find the parallel part of the strain tensor ε_P and its serial part ε_S:

$$\varepsilon_P = P_P : \varepsilon \quad \text{and} \quad \varepsilon_S = P_S : \varepsilon. \tag{4}$$

Hence, the strain state is separated into its parallel and serial part:

$$\varepsilon = \varepsilon_P + \varepsilon_S. \tag{5}$$

The stress state can be separated analogously, finding its parallel and serial parts using the fourth-order tensors P_P and P_S as

$$\sigma = \sigma_P + \sigma_S, \tag{6}$$

where

$$\sigma_P = P_P : \sigma \quad \text{and} \quad \sigma_S = P_S : \sigma. \tag{7}$$

2.1.2. Numerical modeling hypotheses

The numerical model developed to obtain the strain–stress state in the composite is based on the following hypotheses:

(1) The constituent materials of the composite are subjected to the same strain in the parallel (fiber) direction.
(2) Constituent materials are subjected to the same stress in the serial direction.
(3) The response of the composite material is directly related to the volume fractions of its constituent materials.
(4) The phases in the composite are considered to be homogeneously distributed.
(5) The constituent materials are considered to be perfectly bonded.

Although these hypotheses, as well as the serial/parallel mixing theory, can be applied to composites with any number of components, the developed formulation is restricted to only two of them. Therefore, for the sake of consistency, only two composite components will be included in the theory description: fiber and matrix.

2.1.3. Constitutive equations of compounding materials

When applying the serial/parallel mixing theory, it is possible to use any constitutive equation to describe the structural performance of the composite compounding materials. The constitutive equations used can be different for each component (i.e. an elastic law to describe the fiber behavior and a damage formulation to describe the matrix behavior). Considering that additive plasticity is used to formulate the constitutive equations of the materials, the stresses in the matrix and the fiber are obtained as

$$\begin{aligned} {}^{\mathrm{m}}\sigma &= {}^{\mathrm{m}}\mathbb{C} : ({}^{\mathrm{m}}\varepsilon - {}^{\mathrm{m}}\varepsilon^{\mathrm{p}}), \\ {}^{\mathrm{f}}\sigma &= {}^{\mathrm{f}}\mathbb{C} : ({}^{\mathrm{f}}\varepsilon - {}^{\mathrm{f}}\varepsilon^{\mathrm{p}}), \end{aligned} \tag{8}$$

where ${}^{\mathrm{m}}\varepsilon^{\mathrm{p}}$ and ${}^{\mathrm{f}}\varepsilon^{\mathrm{p}}$ are the matrix and fiber plastic-strain tensors, respectively, and ${}^{\mathrm{m}}\mathbb{C}$ and ${}^{\mathrm{f}}\mathbb{C}$ are the matrix and fiber constitutive tensors.

These equations can be rewritten to consider the serial and parallel separation of the strain and stress tensors (Eqs. (5) and (6)):

$$\begin{bmatrix} {}^{i}\sigma_{\mathrm{P}} \\ {}^{i}\sigma_{\mathrm{S}} \end{bmatrix} = \begin{bmatrix} {}^{i}\mathbb{C}_{\mathrm{PP}} & {}^{i}\mathbb{C}_{\mathrm{PS}} \\ {}^{i}\mathbb{C}_{\mathrm{SP}} & {}^{i}\mathbb{C}_{\mathrm{SS}} \end{bmatrix} : \begin{bmatrix} {}^{i}\varepsilon_{\mathrm{P}} - {}^{i}\varepsilon^{\mathrm{p}}_{\mathrm{P}} \\ {}^{i}\varepsilon_{\mathrm{S}} - {}^{i}\varepsilon^{\mathrm{p}}_{\mathrm{S}} \end{bmatrix}, \tag{9}$$

where

$$\begin{cases} {}^{i}\mathbb{C}_{\mathrm{PP}} = P_{\mathrm{P}} : {}^{i}\mathbb{C} : P_{\mathrm{P}} \\ {}^{i}\mathbb{C}_{\mathrm{PS}} = P_{\mathrm{P}} : {}^{i}\mathbb{C} : P_{\mathrm{S}} \\ {}^{i}\mathbb{C}_{\mathrm{SP}} = P_{\mathrm{S}} : {}^{i}\mathbb{C} : P_{\mathrm{P}} \\ {}^{i}\mathbb{C}_{\mathrm{SS}} = P_{\mathrm{S}} : {}^{i}\mathbb{C} : P_{\mathrm{S}} \end{cases} \quad \text{with } i = \mathrm{m}, \mathrm{f}. \tag{10}$$

2.1.4. Equilibrium and compatibility equations

The equations that define the stress equilibrium and establish the strain compatibility between the individual components follow the hypotheses previously described.

Parallel behavior:

$$\begin{aligned} {}^{\mathrm{c}}\varepsilon_{\mathrm{P}} &= {}^{\mathrm{m}}\varepsilon_{\mathrm{P}} = {}^{\mathrm{f}}\varepsilon_{\mathrm{P}}, \\ {}^{\mathrm{c}}\sigma_{\mathrm{P}} &= {}^{\mathrm{m}}k^{\mathrm{m}}\sigma_{\mathrm{P}} + {}^{\mathrm{f}}k^{\mathrm{f}}\sigma_{\mathrm{P}}. \end{aligned} \tag{11}$$

Serial behavior:

$$\begin{aligned} {}^{\mathrm{c}}\varepsilon_{\mathrm{S}} &= {}^{\mathrm{m}}k^{\mathrm{m}}\varepsilon_{\mathrm{S}} + {}^{\mathrm{f}}k^{\mathrm{f}}\varepsilon_{\mathrm{S}}, \\ {}^{\mathrm{c}}\sigma_{\mathrm{S}} &= {}^{\mathrm{m}}\sigma_{\mathrm{S}} = {}^{\mathrm{f}}\sigma_{\mathrm{S}}, \end{aligned} \tag{12}$$

where the superscripts c, m and f stand for composite, matrix and fiber, respectively and ${}^{i}k$ is the volume-fraction coefficient of each constituent in the composite.

2.1.5. Serial/parallel rule of mixtures algorithm

The strain state of the composite material, ${}^{\mathrm{c}}\varepsilon$, at time $t + \Delta t$ is the known variable entered into the algorithm. Using this variable, the serial/parallel rule of mixtures algorithm has to determine the strain and stress states of each component that fulfills the equilibrium, the compatibility and the constitutive equations and the evolution of the internal variables.

The first step of the algorithm is to separate the strain tensor into its parallel and its serial components in order to compute the strain state in the matrix and the fiber. According to Eq. (11), the parallel strain component is the same for both materials and for the composite. However, to determine the serial strain components, it is necessary to predict the expected strains in one of the composite compounding materials. If this prediction is made for the matrix, the algorithm computes its serial strain increment as

$$\left[{}^{\mathrm{m}}\Delta\varepsilon_{\mathrm{S}}\right]^{0} = \mathbb{A} : \left[{}^{\mathrm{f}}\mathbb{C}_{\mathrm{SS}} : {}^{\mathrm{c}}\Delta\varepsilon_{\mathrm{S}} + {}^{\mathrm{f}}k({}^{\mathrm{f}}\mathbb{C}_{\mathrm{SP}} - {}^{\mathrm{m}}\mathbb{C}_{\mathrm{SP}}) : {}^{\mathrm{c}}\Delta\varepsilon_{\mathrm{P}}\right], \tag{13}$$

where $\mathbb{A} = ({}^{\mathrm{m}}k^{\mathrm{f}}\mathbb{C}_{\mathrm{SS}} + {}^{\mathrm{f}}k^{\mathrm{m}}\mathbb{C}_{\mathrm{SS}})^{-1}$ and ${}^{\mathrm{m}}\Delta\varepsilon_{\mathrm{S}} = {}^{t+\Delta t}[{}^{\mathrm{c}}\varepsilon_{\mathrm{S}}] - {}^{t}[{}^{\mathrm{c}}\varepsilon_{\mathrm{S}}]$.

The initial prediction of matrix serial strains, according to the method proposed by Rastellini [15] and shown in Eq. (13), is obtained considering that the parallel and serial components of the total strain are distributed according to the composite stiffness obtained in the previous time step. In the iteration step n, the predicted matrix serial strains are used to compute the fiber serial strains by using Eq. (12). Their expression is

$${}^{t+\Delta t}\left[{}^{\mathrm{f}}\Delta\varepsilon_{\mathrm{S}}\right]^{n} = \frac{1}{{}^{\mathrm{f}}k}\,{}^{t+\Delta t}[{}^{\mathrm{c}}\varepsilon_{\mathrm{S}}] - \frac{{}^{\mathrm{m}}k}{{}^{\mathrm{f}}k}\,{}^{t+\Delta t}[{}^{\mathrm{m}}\varepsilon_{\mathrm{S}}]^{n}, \tag{14}$$

where ${}^{t+\Delta t}[{}^{\mathrm{m}}\varepsilon_{\mathrm{S}}]^{n} = {}^{t}[{}^{\mathrm{m}}\varepsilon_{\mathrm{S}}] + [{}^{\mathrm{m}}\Delta\varepsilon_{\mathrm{S}}]^{n}$.

The next step is to recombine the serial and parallel components of the strain tensor (Eq. (5)). The constitutive equations are then applied to the predicted strains to obtain the stress tensor and the updated internal variables for both materials. The fiber and matrix materials are modeled according to their own constitutive laws. In an

additive plasticity law, Eq. (8) is used to obtain the stress tensor for each one of them. The stresses from the constitutive law must fulfill the following equation:

$$[\Delta\sigma_S]^n = {}^{t+\Delta t}[{}^m\sigma_S]^n - {}^{t+\Delta t}[{}^f\sigma_S]^n \leqslant \text{tolerance}. \tag{15}$$

If the residual stress is smaller than the tolerance, the computed strains and stresses are considered correct and the structural calculation can continue. However, if Eq. (15) is not fulfilled, the initial prediction of the matrix strain tensor has to be corrected. This correction is performed using a Newton–Raphson scheme, which is updated using the Jacobian of the residual forces. The Jacobian is obtained deriving the residue function with respect to the unknown. According to Rastellini [16], the expression for the Jacobian is given as follows:

$$\mathbb{J} = \left.\frac{\partial \Delta\sigma_S}{\partial {}^m\varepsilon_S}\right|_{{}^m\varepsilon_S = {}^{t+\Delta t}[{}^m\varepsilon_S]^n} = [{}^m\mathbb{C}_{SS}]^n + \frac{{}^m k}{{}^f k}[{}^f\mathbb{C}_{SS}]^n \tag{16}$$

and the expression for correcting the matrix serial strains becomes

$${}^{t+\Delta t}[{}^m\varepsilon_S]^{n+1} = {}^{t+\Delta t}[{}^m\varepsilon_S]^n - \mathbb{J}^{-1} : [\Delta\sigma_S]^n. \tag{17}$$

The Jacobian must be obtained using the tangent constitutive tensor for the fibers and the matrix in order to reach quadratic convergence in the serial/parallel mixing theory. However, depending on the constitutive equation defined for each material, it is not always possible to obtain an analytical expression for this tensor. Therefore, in order to obtain a reliable algorithm, the tangent constitutive tensor is computed with a numerical derivation.

2.2. Finite element code

PLCd [17] is a finite element code that works with two and three-dimensional solid geometries. It can deal with kinematic and material nonlinearities. It uses various constitutive laws to predict the material behavior (elastic, visco-elastic, damage, damage-plasticity, etc. [18]) and uses different yield surfaces to control their evolution (Von-Mises, Mohr–Coulomb, improved Mohr–Coulomb, Drucker–Prager, etc. [19,20]). The Newmark method [21] is used to perform dynamic analysis. A more detailed description of the code can be obtained from [22,23]. The main numerical features included in the code to deal with composite materials are:

Classical and serial/parallel mixing theory: The classical mixing theory was first developed by Truesdell and Toupin and is based on the iso-strain behavior of composite components [13,14]. Fig. 1 shows how the serial/parallel rule of mixtures algorithm is implemented in the PLCd code.

Anisotropy using a mapped space theory: This theory enables the code to consider materials with a high level of anisotropy, without the associated numerical problems [24,25].

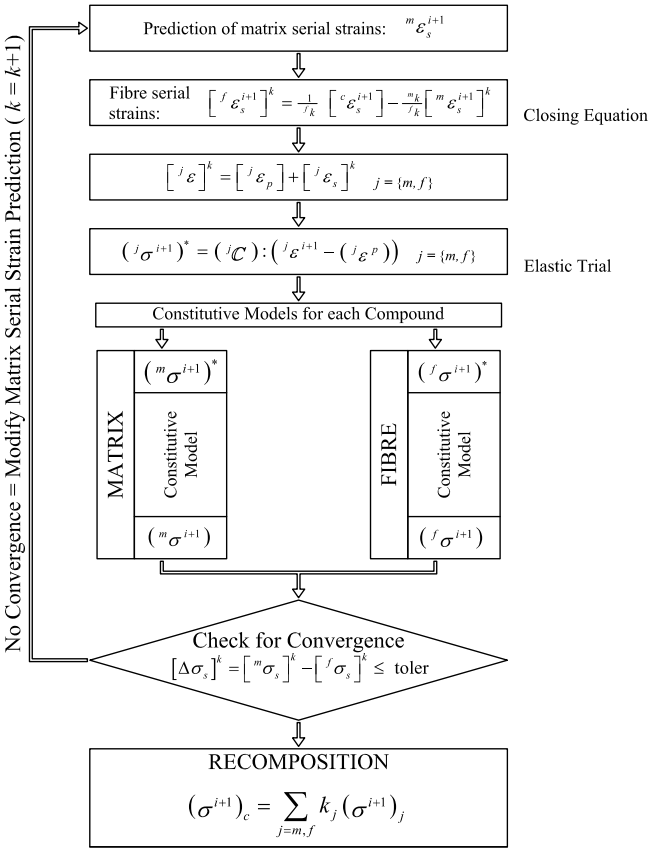

Fig. 1. Flow chart of the serial/parallel rule of mixtures algorithm.

Fiber–matrix debonding: This effect reduces the composite strength due to the failure of the fiber–matrix interface [13,26].

2.2.1. Tangent constitutive tensor

A perturbation method is used to obtain the tangent constitutive tensor, $\mathbb{C}^t$, numerically for each constituent material of the composite. The tangent constitutive tensor is defined as follows:

$$\dot{\boldsymbol{\sigma}} = \mathbb{C}^t : \dot{\boldsymbol{\varepsilon}}. \tag{18}$$

The tangent constitutive tensor can be written for isotropic and orthotropic materials, by reducing the tensors to their matrix description:

$$\begin{bmatrix} \dot\sigma_1 \\ \vdots \\ \dot\sigma_n \end{bmatrix} = \begin{bmatrix} c^t_{11} & \cdots & c^t_{1n} \\ \vdots & \ddots & \vdots \\ c^t_{n1} & \cdots & c^t_{nn} \end{bmatrix} \begin{bmatrix} \dot\varepsilon_1 \\ \vdots \\ \dot\varepsilon_n \end{bmatrix}. \tag{19}$$

The stress vector rate of Eq. (19) can be obtained as the sum of n stress vectors, which are the product of the j component of the strain vector rate and the j column of the tangent stiffness tensor. This is

$$\dot{\boldsymbol{\sigma}} \equiv \sum_{j=1}^{n} \delta^j \boldsymbol{\sigma} = \sum_{j=1}^{n} \mathbf{c}^t_j \cdot \dot\varepsilon_j \tag{20}$$

with

$$\mathbf{c}_j^t = [\, c_{1j}^t \quad c_{2j}^t \quad \cdots \quad c_{nj}^t \,]^{\mathrm{T}}. \tag{21}$$

Eq. (20) can be used to obtain the j column of the tangent stiffness tensor, which is unknown:

$$\mathbf{c}_j^t = \frac{{}^j\dot{\boldsymbol{\sigma}}}{\dot{\varepsilon}_j} \equiv \frac{\delta^j\boldsymbol{\sigma}}{\delta\varepsilon_j}. \tag{22}$$

The perturbation method consists in defining n small variations, or perturbations, of the strain vector $\delta\varepsilon_j$, to obtain n stress vectors $\delta^j\boldsymbol{\sigma}$ that will be used in Eq. (22) to obtain the numerical expression of the tangent constitutive tensor.

2.2.2. Numerical implementation of the tangent constitutive tensor

In a finite element code the material constitutive law provides the stress tensor $\boldsymbol{\sigma}$ and the internal variables q associated with a defined strain tensor $\boldsymbol{\varepsilon}$. With the strain and stress vectors resulting from the constitutive equation, a small perturbation is applied to the strain vector to obtain its associated stress tensor. The obtained stresses and the defined perturbation are then used to compute the tangent constitutive matrix as shown in Eq. (22). Fig. 2 shows the flow chart of the algorithm implemented in PLCd code.

In the procedure proposed, the smaller the perturbation value the better the approximation of the tangent constitutive tensor. With this consideration in mind, the perturbation value defined for each component of the strain tensor is obtained by applying the following procedure:

$$\begin{aligned} &\text{if } \varepsilon_j \neq 0 \;\rightarrow\; \delta\varepsilon_j = \varepsilon_j \cdot 10^{-5}, \\ &\text{if } \varepsilon_j = 0 \;\rightarrow\; \delta\varepsilon_j = \min\{\varepsilon_k\} \cdot 10^{-5} \quad \forall k = 1, n. \end{aligned} \tag{23}$$

Selecting the perturbation value by using this method, the strain increment will always be small enough to ensure that the stress variation is close to the computed value. However, this procedure can provide perturbation values close to zero (i.e. when one of the strain values is almost zero). This case will lead to an indetermination in Eq. (22). To prevent this problem from arising, the following condition is imposed to ensure that the perturbation value is sufficiently high:

$$\delta\varepsilon_j > \max\{\varepsilon_k\} \cdot 10^{-10} \quad \forall k = 1, n. \tag{24}$$

This procedure provides an accurate approximation of the tangent constitutive tensor for any constitutive law used and any yield surface; and ensures that the numerical process converges satisfactorily.

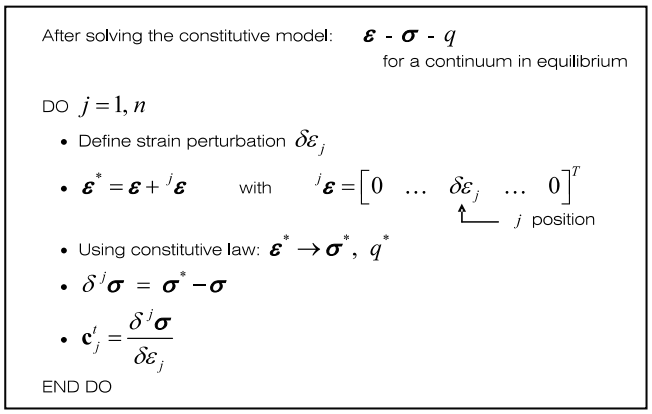

Fig. 2. Flow chart of the perturbation method algorithm for obtaining the tangent constitutive tensor.

2.3. Retrofitted structures. Construction-stages algorithm

There are many situations in which an existing structure can be damaged and can require to be retrofitted. The damage in the structure can be caused by several reasons, such as a collision [27] or after an earthquake [28]. Therefore, structural retrofitting is probably one of the main applications of CFRP in civil engineering structures.

In order to simulate a structural retrofitting, it is necessary to add the CFRP reinforcement once the structure is already damaged. With this aim, a construction-stages algorithm is implemented in the PLCd code [17], so that it is possible to add or remove structural elements during the calculation process.

This algorithm enables the code to run the numerical simulation for the desired load cases, with only some structural elements active in the structure. Being possible to add new elements at a given load case, without interrupting the calculation process. These elements must be free from strains and stresses when they are activated.

Fig. 3 shows how this solution scheme is used when simulating a retrofit process. The example shown corresponds to a beam to which a bending moment is applied. The beam is reinforced with CFRP when the first tensile cracks appear on the bottom edge.

The finite element method is based on the numerical integration of the virtual work equation; this integration implies to solve the problem:

$$KX = R, \tag{25}$$

where K is the global stiffness matrix, X is the vector of nodal displacements and R is the vector of external forces applied to the structure. Once the nodal displacements have been found, the strains in each element, ε^{e}, are computed using the following equation:

$$\varepsilon^{\mathrm{e}} = B^{\mathrm{e}} X^{\mathrm{e}}, \tag{26}$$

where B^{e} is the element deformation matrix.

Finally, once the element strains have been obtained, the following equation is used to compute the stresses in each element:

$$\sigma^{\mathrm{e}} = \mathbb{C}^{\mathrm{e}} \varepsilon^{\mathrm{e}}, \tag{27}$$

where $\mathbb{C}^{\mathrm{e}}$ is the element constitutive matrix.

The stress tensor in Eq. (27) corresponds to the elastic stresses. This expression is modified in a material nonlinear

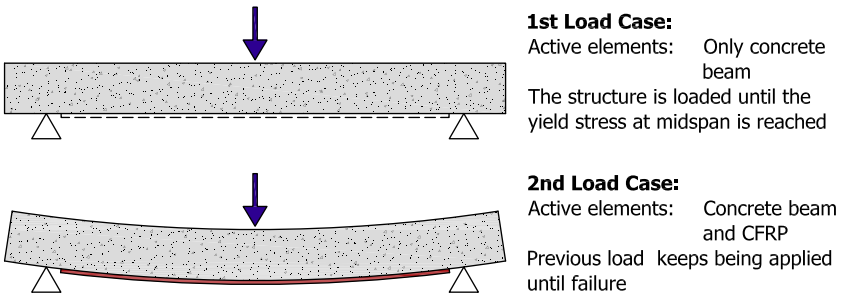

Fig. 3. Retrofit process of a beam with a bending moment.

analysis. However, for the sake of simplicity, the explanation of the procedure is limited to the linear case.

Considering that there are n load cases in the calculation process, Eqs. (26) and (27) can be rewritten as

$$\begin{aligned}\varepsilon^{e} &= \varepsilon_1^{e} + \varepsilon_2^{e} + \cdots + \varepsilon_n^{e} = B^{e}X^{e},\\ \sigma^{e} &= \sigma_1^{e} + \sigma_1^{e} + \cdots + \sigma_n^{e} = \mathbb{C}^{e}\varepsilon^{e}.\end{aligned} \tag{28}$$

If new elements are introduced into the structural mesh during finite element analysis (i.e. in the second load case), they will take values of $\varepsilon_1^{e} = 0$ and $\sigma_1^{e} = 0$; and the strains in the element will correspond only to the second load case:

$$\varepsilon^{e} = \varepsilon_2^{e} = B^{e}X^{e}. \tag{29}$$

However, the element displacement introduced in Eq. (29) corresponds to the total displacement of the structure. This means that the strains in the new element correspond to the displacements of the structure during the first and the second construction stages. The same applies to the stress tensor. Consequently, the new elements try to adapt to the global deformation of the structure by adopting strains that are greater than the ones that correspond to the new load increase.

By considering all of the structural elements during all construction stages, it is possible to prevent this situation. Then, it is necessary to separate the strain tensor into two components, one active (ε_{A}) and one non-active ($\varepsilon_{\mathrm{NA}}$), that is

$$\varepsilon^{e} = \varepsilon_{\mathrm{A}}^{e} + \varepsilon_{\mathrm{NA}}^{e}. \tag{30}$$

When the element is not present in the structure, all strains are included in the non-active tensor:

$$\varepsilon^{e} = \varepsilon_{\mathrm{NA}}^{e} = B^{e}X^{e} \quad \text{and} \quad \varepsilon_{\mathrm{A}}^{e} = 0 \tag{31}$$

and if the element is active, Eq. (30) is used to calculate its strain tensor:

$$\varepsilon_{\mathrm{A}}^{e} = \varepsilon^{e} - \varepsilon_{\mathrm{NA}}^{e} = B^{e}X^{e} - \varepsilon_{\mathrm{NA}}^{e}. \tag{32}$$

With this procedure, only the strains that correspond to the construction stage in which the element is active are considered.

Element stresses are computed by considering only the active strains:

$$\sigma^{e} = \mathbb{C}^{e}\varepsilon_{\mathrm{A}}^{e}. \tag{33}$$

Thus, no stresses are obtained if the element is non-active.

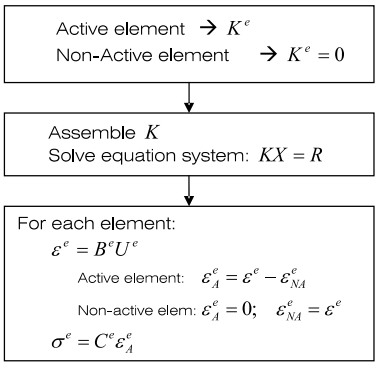

Fig. 4. Flow chart of the construction-stages algorithm.

This procedure has been implemented in the PLCd code and it provides correct results, as shown in the beam test described in Section 4 of this paper.

The algorithm must take into account that the elemental stiffness matrices (K^{e}) of any non-active elements present in the structure are included in the global stiffness matrix K. As a result, these elements contribute to the global stiffness of the structure. The elemental stiffness matrices of the non-active elements should therefore be nullified at the beginning of the construction stage to prevent this contribution from affecting the results.

Fig. 4 shows a flow chart of the construction-stages algorithm implemented in the PLCd code.

3. Validation of the numerical procedure

To validate the proposed formulation, a numerical model of a RC beam reinforced with FRP was developed. The beam considered is the same as the one defined by Spadea et al. in [2]. The numerical results obtained with PLCd are compared with the experimental results given in [2].

3.1. Beam and model description

The structure used to validate the code is a simply supported beam to which two equidistant loads are applied, which produces a constant bending moment between them. Fig. 5 shows the beam geometry and the reinforcement added to it.

The experimental simulations reported in [2] consist in using a displacement-control mechanism to apply a load

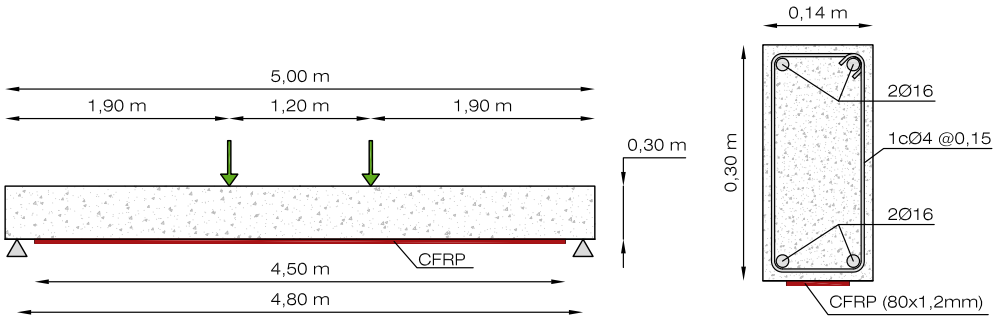

Fig. 5. Geometric definition of the studied beam.

until the beam fails. Different CFRP reinforcement configurations are applied to the beam to obtain the force–displacement response for each one. Two of these results are used to validate the proposed numerical model: the first is for the non-reinforced beam and the second is for the beam with the CFRP reinforcement displayed in Fig. 5. The reinforcement applied is 1.2 mm thick and composed of 66% of carbon fibers, oriented along the longitudinal axis of the beam, and 34% of polymeric matrix. The experimental results are compared with the numerical results for the developed models. These are:

Sp3D-R0: Beam without CFRP reinforcement.
Sp3D-R1: Beam with bending CFRP reinforcement.

The constitutive performance of each composite material used to simulate the beam is determined by combining the constitutive behaviors of their constituent materials. Table 1 shows the simple materials considered in the models and their mechanical characteristics. In this table, E stands for the Young modulus, ν for the Poisson modulus, σ_C and σ_T for the yielding compression and tension stresses, respectively, and G_C and C_T for the energy release rates per unit area in compression and tension.

Concrete and matrix are simulated by a damage formulation. Steel and carbon fibers are simulated by a plastic law. Young's modulus of steel has been reduced to take into account the effect of fiber debonding [29]. Steel plastic evolution is defined by an initial hardening law until it reaches a peak of 435 MPa, at which point the hardening law is replaced by a softening law. Fig. 6 shows the strain–stress evolution of each material considered in the simulation in the case of tensile stresses.

The numerical models developed in this article are based on hexahedral elements. Six different composite materials

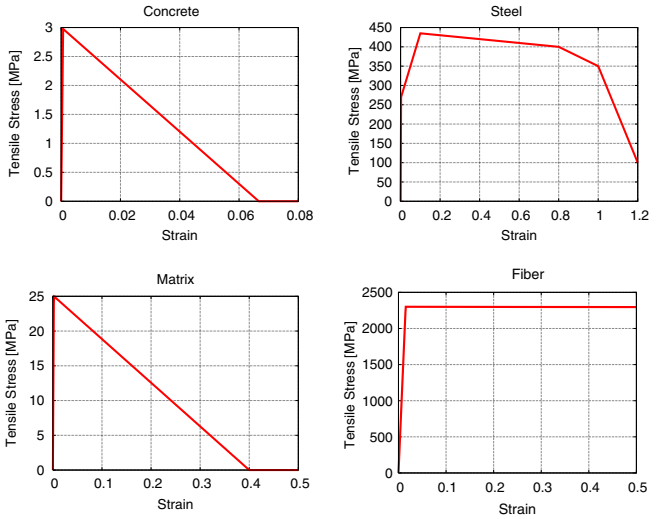

Fig. 6. Strain–stress evolution of each constituent material considered in the analysis.

are defined by a combination of six different constituents: concrete, matrix, fibers and three steel materials. Different steel materials are defined according to their orientation because the direction of the fibrous material is required as a material property in the serial/parallel mixing theory. Transversal and vertical steel refer to the steel stirrups and longitudinal steel refers to the bending steel reinforcement.

Table 2 contains the definitions of each composite material according to the volumetric participation of their constituents. Fig. 7 shows the distribution of these materials in the beam model and the mesh defined for the simulation. Only half of the beam has been modeled because of the symmetry at mid-span. The figure also shows that complex material distributions in the cross-section of the beam can

Table 1
Mechanical characteristics of the constituent materials defined in the beam models

Material	Yielding criterion	E (MPa)	ν	σ_C (MPa)	σ_T (MPa)	G_C (kJ/m^2)	G_T (kJ/m^2)
Concrete	Mohr–Coulomb	2.5×10^4	0.2	30.0	3.0	5.0	0.5
Steel	Von-Mises	1.0×10^5	0.0	270	270	2000	2000
Polymeric matrix	Mohr–Coulomb	1.2×10^4	0.2	87.5	25.0	10.5	3.0
Carbon fibers	Von-Mises	1.5×10^5	0.0	2300	2300	2000	2000

Table 2
Definition of composite materials. Volumetric participation of each constituent material in the composite

Constituent materials	Composite materials					
	Mat-01	Mat-02	Mat-03	Mat-04	Mat-05	Mat-06
Concrete	1.00	0.57	0.99	0.98	0.99	
Longitudinal steel		0.42				
Transversal steel				0.01	0.01	
Vertical steel		0.01	0.01	0.01		
Polymeric matrix						0.34
Long. carbon fibers						0.66

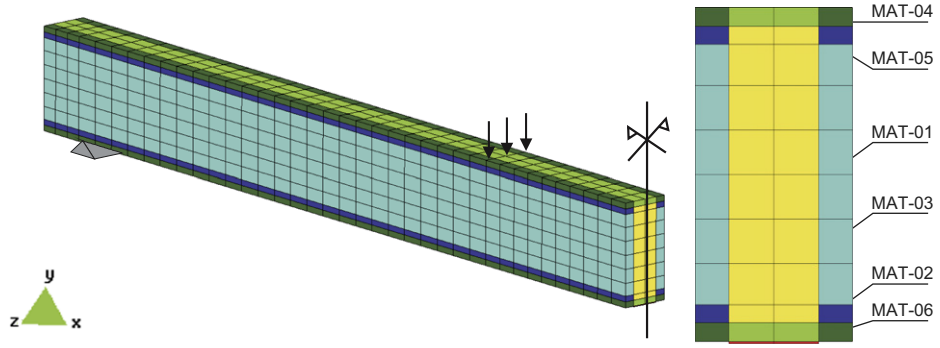

Fig. 7. Definition of the mesh and composite materials of the simulated beam. The model assumes symmetry at mid-span.

be considered using the serial/parallel mixing theory, without having to model each single element independently.

3.2. Results

The force–displacement curves (capacity curves) obtained in each case (Fig. 8) are used to compare the numerical and experimental models. The displacement corresponds to the point at which the load is applied. The agreement between the results is good enough to indicate that the code works properly.

The agreement between the experimental and numerical results can be observed not only in the structural response of the beam but also in its failure mode. The failure modes reported by Spadea et al. are:

No reinforced beam: Tension steel yielding and concrete crushing.
Reinforced beam: Sudden and total loss of load capacity; explosive debonding of CFRP plate.

The failure mode in the non-reinforced beam model (Sp3D-R0) is the same as the one obtained in the experimental test. This can be seen in Figs. 9 and 10, which show the damage to the concrete and the plastic damage to the steel reinforcement for the final calculation step and for the most severely damaged beam section. These figures show that the steel has started to yield and that the compressed concrete has also reached its limit stress (onset of

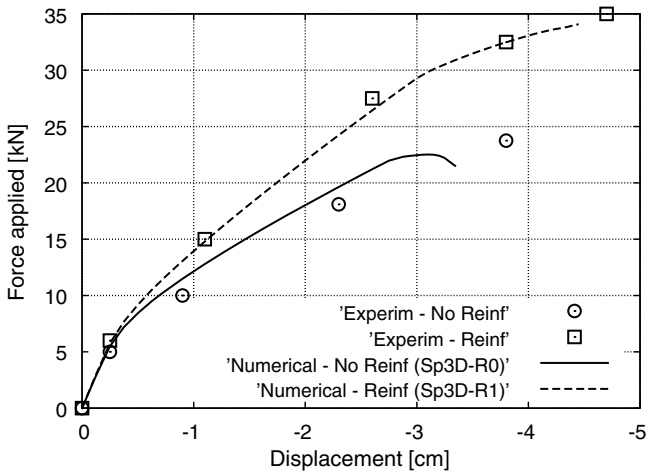

Fig. 8. Comparison between numerical and experimental capacity curves.

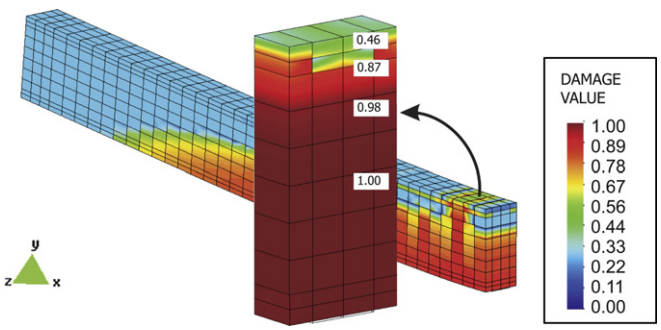

Fig. 9. Damage to the concrete at beam failure and detail of the most severely damaged cross-section. The numbers shown correspond to the damage parameter in each finite element. Sp3D-R0 model.

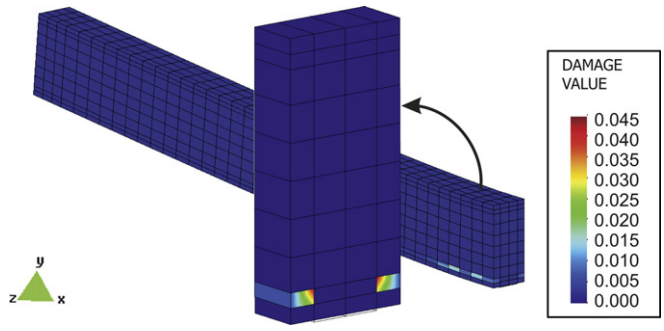

Fig. 10. Plastic damage to the steel at beam failure and detail of the most severely damaged cross-section. Sp3D-R0 model.

concrete crushing). Under these conditions the transversal section cannot develop more stresses and the code cannot determine a valid solution for the current load step. This situation can be interpreted as beam failure.

The failure mode of the CFRP reinforced beam model (Sp3D-R1) is similar to that of the non-reinforced beam model (Sp3D-R0). In the most severely damaged section the entire concrete reaches its elastic limit stress and the steel yields (Fig. 11). The developed model assumes a perfect bond between the concrete and the reinforcement. Under this assumption, it is impossible to simulate the explosive debonding of the CFRP plate observed in the experimental test. However, if debonding occurred, the beam would suddenly lose load capacity and the results would be identical to the experimental ones.

CFRP reinforcement increases the tensile strength of the beam and reduces the crack opening, which increases the load capacity of the beam. Crack opening increases exponentially in the most severely damaged section of the non-reinforced beam model (Sp3D-R0) when steel yielding begins. This increase is not observed when the beam is reinforced with CFRP. This can be seen in Fig. 12 which shows the relative displacement between the nodes found on either side of the most severely damaged section in both models. The strength is increased and crack opening is reduced because the carbon fibers are still under elastic conditions; in fact, they are at less than 30% of their elastic

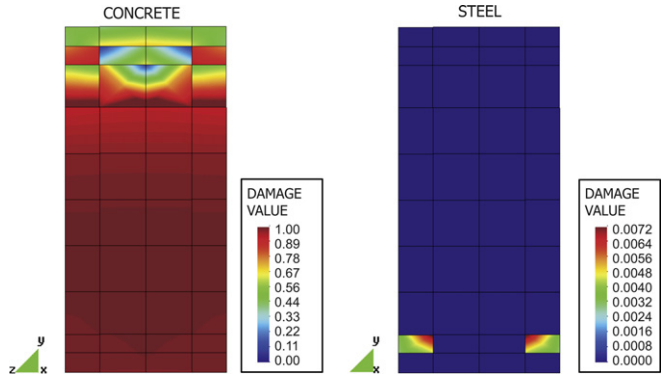

Fig. 11. Damage at the cross-section supporting heavier loads at beam failure. Sp3D-R1 model.

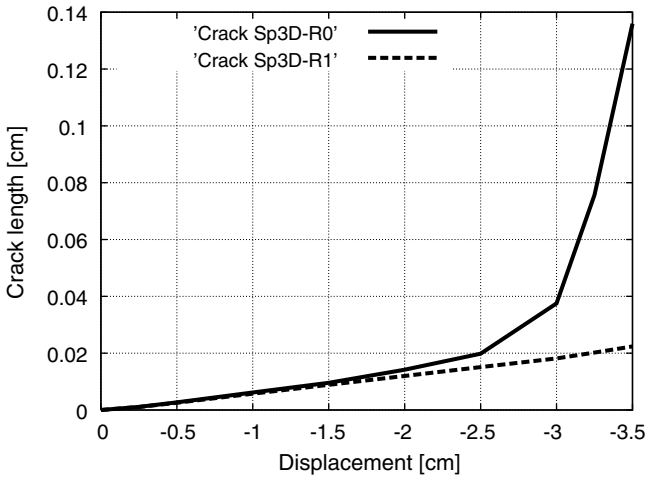

Fig. 12. Crack opening in the most severely damaged section.

capacity, although damage has already started to appear in the polymeric matrix (Fig. 13).

3.3. S/P mixing theory performance

The models developed for validating the code are also used to study the performance of the serial/parallel mixing theory. Fibrous materials work in their longitudinal direction, consequently, the stresses should be greater in this direction. The serial/parallel mixing theory should simulate this behavior. To verify this, the performance of steel stirrups is studied herein. Beam strains in transversal direction tend to increase in the upper bound of the cross-section and to decrease in its lower bound due to Poisson effects. Concrete confinement reduces this effect by means of steel stirrups. Fig. 14 shows the transverse stresses in the stirrups, which correspond to stresses in the longitudinal direction of the stirrups. This demonstrates that the model is capable of simulating the confinement of the concrete.

The serial/parallel rule of mixtures is providing correct results if the global longitudinal stresses in the stirrups (transversal stresses according to their orientation) are the same as in the concrete. This situation is achieved, as shown in Fig. 15. Moreover, steel stresses in the longitudinal direction of the beam are lower than the stresses found in the transverse direction (which corresponds to the orientation of the studied stirrups).

4. CFRP retrofitting of RC structures

Two different numerical models have been developed to study the effect of retrofitting a structure, depending on the existing level of damage in the beam when the CFRP reinforcement is applied. The beam retrofitted is the same that has been used in previous section. The models developed are:

Sp3D-Rt2: The CFRP reinforcement is applied when the damage appears in the concrete material.

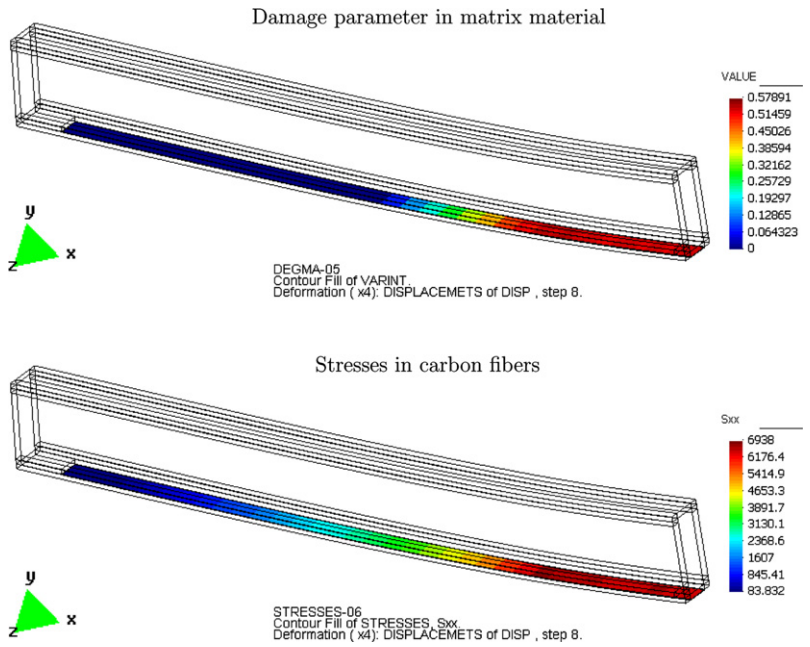

Fig. 13. Stress state in CFRP reinforcement. Sp3D-R1 model.

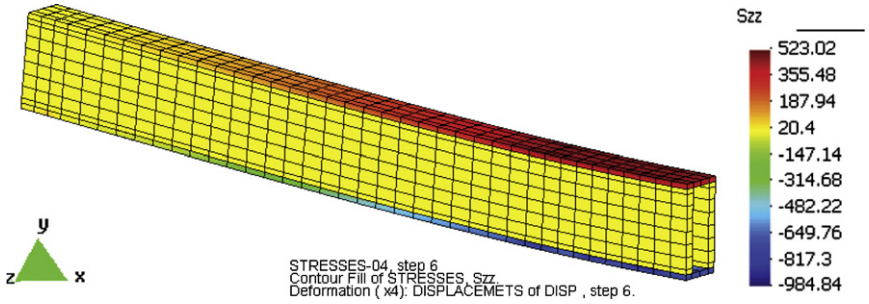

Fig. 14. Transverse stresses in transverse steel stirrups. Sp3D-R0 model.

Sp3D-Rt3: CFRP reinforcement is applied when the steel starts to yield.

Results obtained with these two models are compared with those obtained when the beam is not reinforced (Sp3D-R0 model) and when the beam is reinforced from the beginning of the loading process (Sp3D-R1 model). Fig. 16 shows the capacity curves for each model.

These results show that the structural stiffness does not depend on the point at which the reinforcement is applied to the structure. The structural stiffness obtained when the CFRP reinforcement is applied after the steel has begun to yield (Sp3D-Rt3) does not differ significantly from the structural stiffness obtained after steel yielding in the reinforced model (Sp3D-R1). However, Fig. 16 also shows that retrofitted structures suffer greater deformation and damage than structures that are reinforced during the original construction. The resulting damage reduces the load capacity of the beam and the deformation can lead to a loss of serviceability (i.e. when a load of 25 kN is applied to the structure), the beam deformations are 45% greater in the retrofit model Sp3D-Rt3, than in the reinforced model Sp3D-R1.

5. Concrete frame structure simulation

The main aim of this simulation is to apply the formulation developed to verify the ability of CFRP reinforcements to increase the strength of concrete frame structures. The connecting joints between the beams and columns can be often subject to greater stress than other zones of concrete frame structures and in most cases these joints are the cause of structural weakness. The frame joint is reinforced in the models developed for this study with two different CFRP configurations to analyze the strength mechanisms developed by the reinforcement to increase the frame strength and to determine which type of reinforcement configuration yields better results.

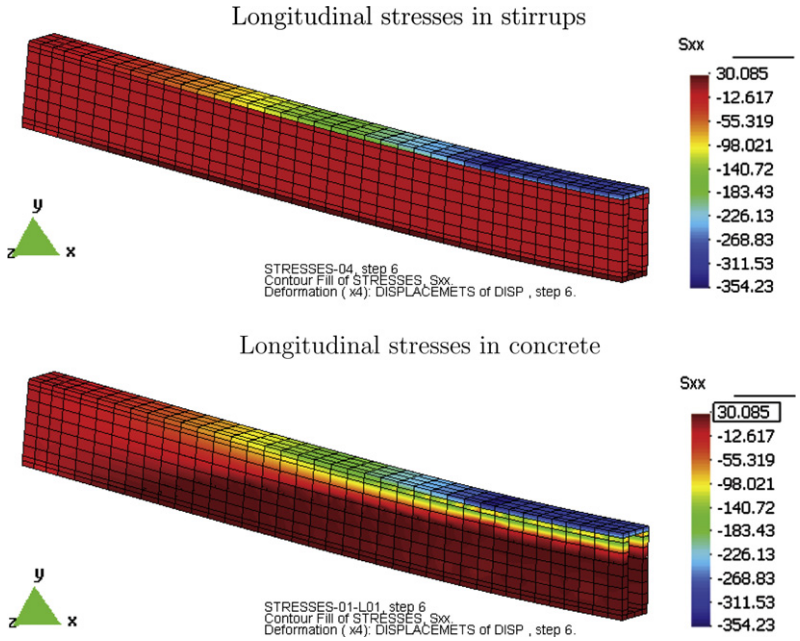

Fig. 15. Longitudinal stresses in concrete and in steel stirrups. Sp3D-R0 model.

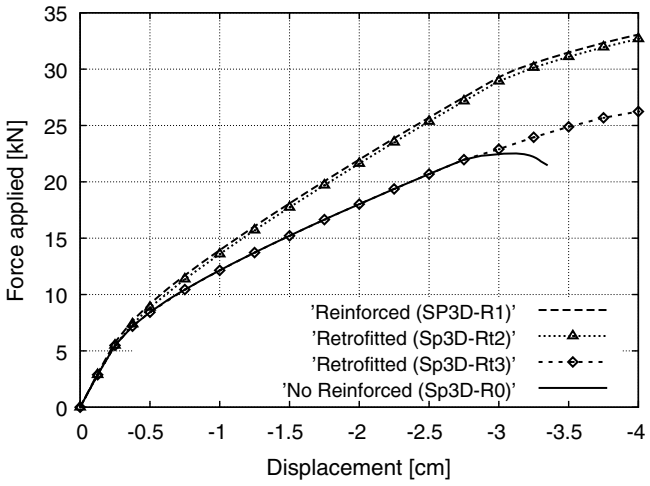

Fig. 16. Comparison of CFRP reinforcements and retrofitting using capacity curves.

5.1. Model description

The concrete frame to be studied is designed to reflect the most common geometry and steel reinforcements used in this type of construction. Fig. 17 shows the geometry considered and Fig. 18 shows the steel reinforcement and the CFRP reinforcement that will be applied to the frame joint. The dimensions of the cross-section of the beam and the steel reinforcement are intended to ensure structural failure close to the joint. The height of the beam is smaller than the width and less steel reinforcement is used for the beam than for the column. This will increase the effect of the CFRP on in the frame joint. The structure is loaded by a horizontal force P applied in the middle of the frame joint (see Fig. 17).

Two-dimensional and three-dimensional models have been developed for the concrete frame. The 2D models have been used to calibrate the mesh, as they require less computational effort than the 3D models. Results obtained with the 2D models are compared with those of the 3D models to assess the accuracy of each type of simulation. Three different structure models have been developed to study the effect of CFRP reinforcements on the frame joint:

2DF-noR and 3DF-noR models: Two- and three-dimensional models of the concrete frame without CFRP reinforcement.
2DF-R and 3DF-R models: Two- and three-dimensional models of the concrete frame with upper and lower CFRP reinforcements.
2DF-LR and 3DF-LR models: Two- and three-dimensional models of the concrete frame with upper, lower and lateral CFRP reinforcements.

The constituent materials of the different composites in each model are the same as those defined for the beam (Table 1). The CFRP reinforcement is 1.2 mm thick and is composed of 66% of carbon fibers and 34% of polymeric matrix. The fibers in the upper and lower reinforcements are aligned with the longitudinal axis of the structure. Two layers are applied to the frame to provide lateral reinforcement, in which the fibers are oriented at +0° and +90° with respect to the horizontal.

5.2. 2D results

The capacity curves obtained for each model (Fig. 19) are used to analyze the structural behavior of the frame joint with the different types of reinforcement. The x-axis

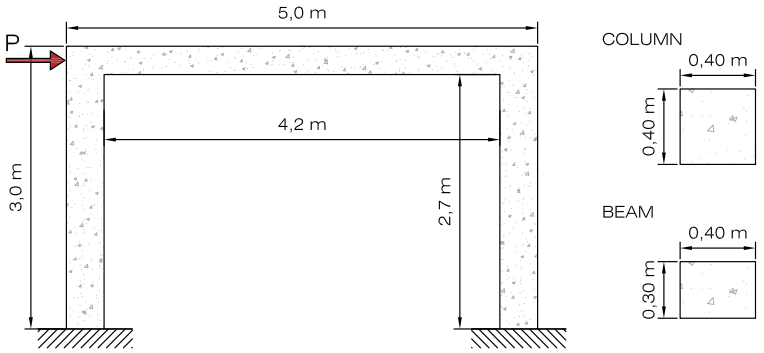

Fig. 17. Geometric definition of the frame.

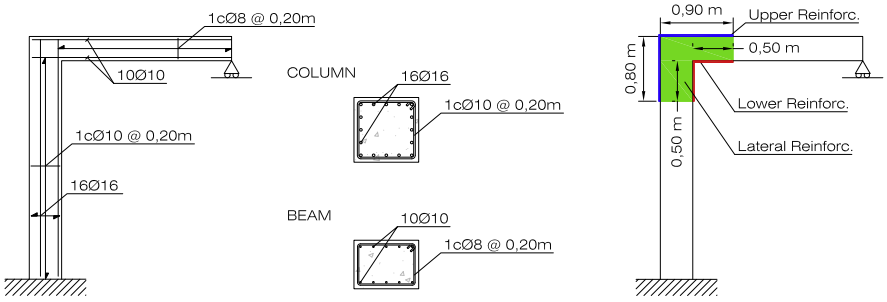

Fig. 18. Reinforcements of the concrete frame.

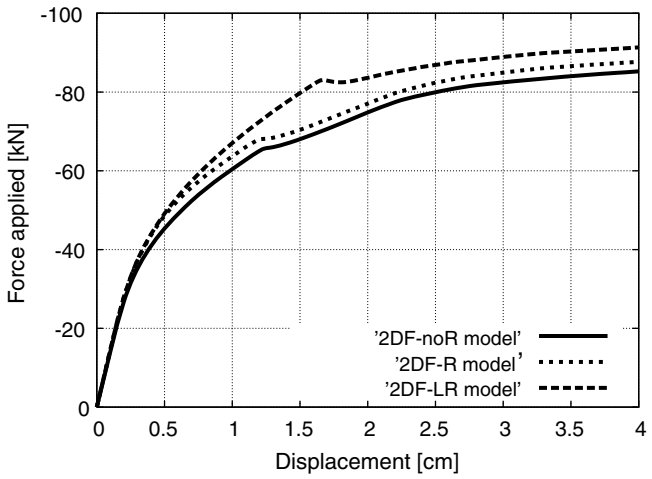

Fig. 19. Capacity curves obtained with the 2D models.

shows the horizontal displacement of the point to which the load is applied and the *y*-axis shows the load applied. The displacement depends on the column, the beam and the joint stiffness. Any increase in the structure stiffness shown by the force–displacement graph will reflect an increase of the joint stiffness as a result of the CFRP reinforcement because the column and the beam are not modified in the different models.

Fig. 19 shows that the upper and lower CFRP reinforcements (2DF-R model) do not significantly improve the frame behavior. A substantial improvement is only found when the lateral reinforcement is applied to the concrete frame. All three curves contain a region in which the load is reduced, after which it begins to increase again. These points reflect the point at which a plastic hinge develops in the structure. The structure adopts a new strength mechanism at this load step, which increases its load capacity. If the load applied to the structure when the plastic hinge is developed is considered, results show that the lateral reinforcement (2DF-LR model) increases the structural load capacity by 25%, when compared with the non-reinforced model (2DF-noR). This increase is reduced to 4% if the structure is only reinforced with upper and lower CFRP.

The effects of each type of reinforcement can be better understood by studying the points at which the plastic hinges are formed. Fig. 20 shows the longitudinal strains for each model at the last computed step. The cross-sections in which the plastic hinges are formed are subjected to the greatest strain.

Fig. 20 shows the plastic hinge moves from the beam to the inner part of the joint, where no reinforcement is applied if only the upper and lower CFRP reinforcements are included into the structure. Therefore, the upper and lower CFRP reinforcement does not change the beam behavior substantially; once the hinge has been formed, both structures behave similarly (Fig. 19). On the other hand, when the lateral reinforcement is applied to the structure, it limits damage in the frame joint and causes the plastic hinge to move to the cross-section at which no CFRP reinforcement is applied. This increases the load capacity and the stiffness of the structure.

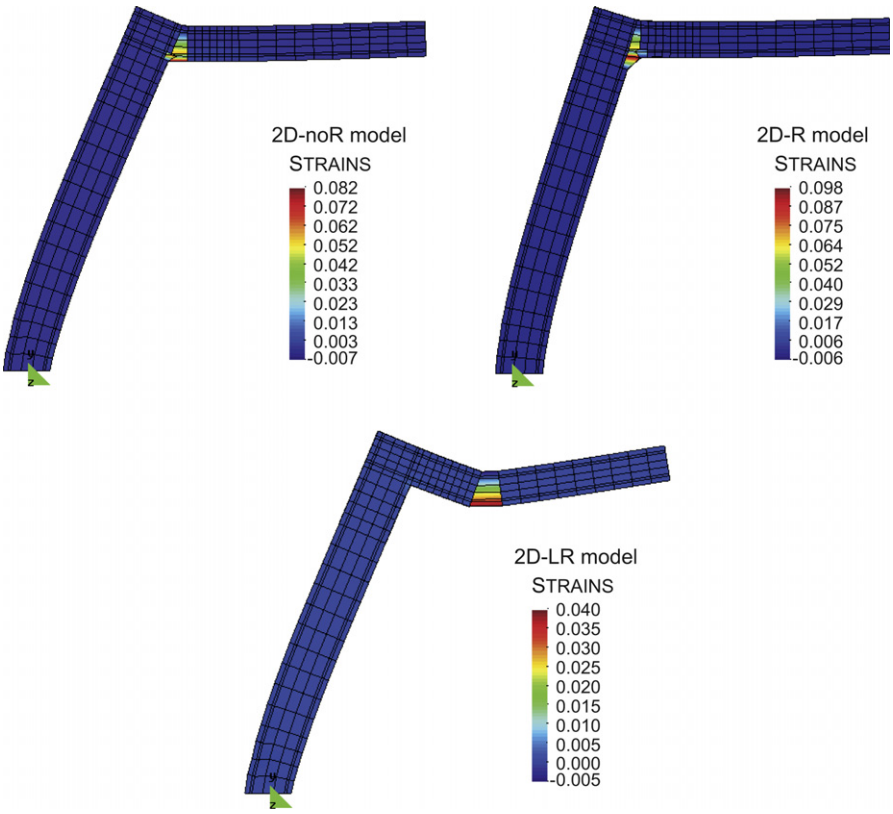

Fig. 20. Plastic hinges in the concrete frame. 2D models.

5.3. 3D results

The capacity curves are also used to analyze the results obtained with the 3D models (Fig. 21). The main difference between the 3D and the 2D results is that the 3D models are stiffer and can support greater maximum loads than the 2D models. This is due to the fact that the concrete confinement is reproduced more accurately by the 3D models because the steel stirrups are modeled taking into account their 3D distribution rather than only one of their dimen-

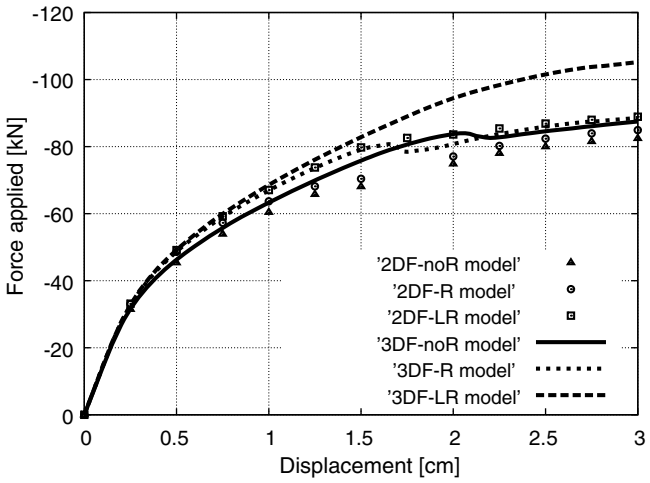

Fig. 21. Capacity curves obtained with the 3D models.

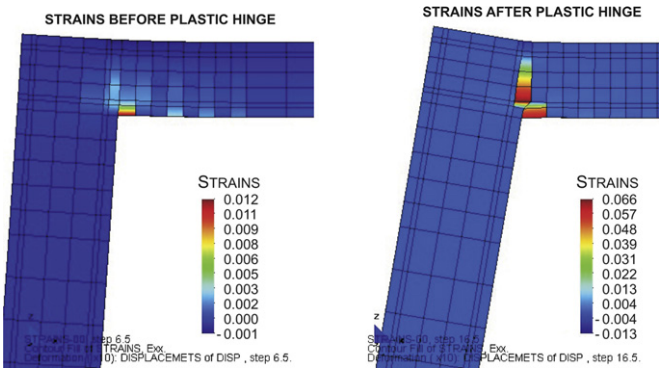

Fig. 22. Crack evolution in the 3DF-noR model.

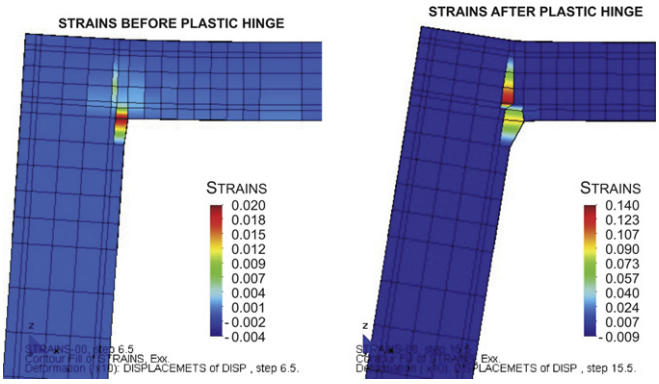

Fig. 23. Crack evolution in the 3DF-R model.

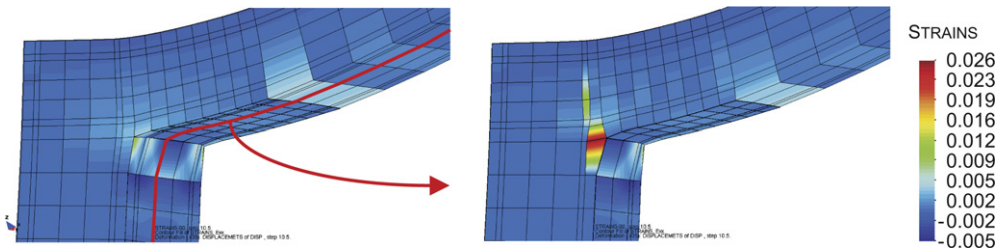

Fig. 24. Plastic hinge in 3DF-LR model. Lateral view.

sions. This confinement enables the concrete to support greater longitudinal stresses and slows the spread of damage. Both of these improvements increase the strength and stiffness of the structure.

Fig. 21 shows that the plastic hinges appear at the same load and displacement in the 3D non-reinforced model (3DF-noR) and in the upper and lower reinforced model (3DF-R) as in the 2D lateral reinforced model (2DF-LR), due to the increased strength of the concrete. However, the plastic hinges appear earlier in the reinforced model than in the non-reinforced one in the three-dimensional simulation. This effect is illustrated by Fig. 22, which shows the maximum strains in the non-reinforced beam model (3DF-noR) before and after the formation of the plastic hinge, and Fig. 23, which shows the same results for the upper and lower reinforced model (3DF-R).

These figures show that the plastic hinge develops in almost the same cross-section in both models. However, since this cross-section is closer to the initial point of damage in the upper and lower reinforced model than in the non-reinforced model, the code finds faster the crack path in the reinforced case. Therefore, although CFRP reinforcement increases the joint stiffness, in this case the load that causes the plastic hinge to appear is lower when the joint is reinforced than when no reinforcement is applied.

More differences are found when the three-dimensional model is compared with the two-dimensional model for the case in which lateral CFRP reinforcement is applied to the frame joint (3DF-LR model). The first difference is that the capacity curve does not show the formation of a plastic hinge. This is because no section is completely damaged when the code no longer converges.

However, the main difference can be observed in the most severely damaged section. The strains in the lateral sections of the frame joint (Fig. 24a) are similar to the one seen in the 2D case: they are greater in the cross-section where the CFRP reinforcement ends than in the frame joint. Although, when the strains in a longitudinal section of the structure are analyzed (Fig. 24b), it can be seen that the plastic hinge is developed in the frame joint. Two-dimensional models assume that the CFRP reinforcement is applied through the entire cross-section whereas it is only applied to the lateral surfaces. Consequently, the reinforcement can prevent structural cracks from appearing on the surface of the frame joint but cannot protect the inside of the joint. This effect can be seen more clearly in Fig. 25,

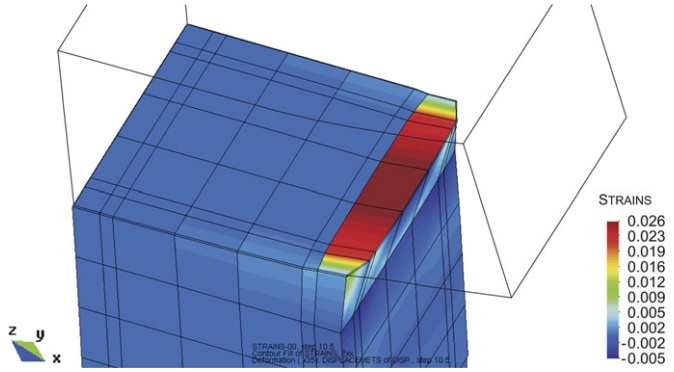

Fig. 25. Elements with larger deformations in 3DF-LR moldel. Top view.

which shows a top view of the strains in the column section just below the frame joint.

These last two figures show that same structural failure occurs regardless of the CFRP reinforcement configuration applied. Therefore, it can be concluded that lateral CFRP reinforcement does not prevent the appearance of cracks in the joint and the subsequent formation of a plastic hinge, but it can delay the load step during which the first cracks appear and reduce the speed with which they propagate. These both effects increase the load of the frame by 20% when the horizontal displacement is 3.0 cm, which makes this type of reinforcement the optimum for strengthening the column–beam joint of concrete frame structures.

6. Conclusions

The results of the numerical procedures and simulations developed in this paper show that the numerical tool developed to simulate FRP reinforcements of RC structures performs well. The results are in good agreement with existing experimental results. The code is prepared to compute real structures that are reinforced or retrofitted with CFRP. Last simulation presented has shown that different numerical simulations with different FRP reinforcements can be performed with PLCd in order to obtain the most suitable reinforcement configuration for the problem under study.

It has been proved that the serial/parallel rule of mixtures can obtain the composite performance by combining the mechanical behavior of its different constituents, each one computed with its own specific constitutive equation. The theory takes into account the directional behavior of the fiber constituents.

The construction-stages algorithm has shown how important is to reinforce the structure when a low level of damage is observed. Even if the structure stiffness does not vary if FRP is applied for reinforcement or retrofitting, the structural deformations and the stresses are greater if FRP is applied when the structure is already damaged.

The frame simulations have shown that it is necessary to use three-dimensional elements to correctly simulate the behavior of the structure. Using two-dimensional elements implies assuming that the materials are evenly distributed through the cross-section. However, this assumption can cause overestimation of the structural performance if the structural components are not evenly distributed, as is the case with the lateral reinforcements in the 2D frame structure simulation. Nevertheless, if the condition of an evenly distribution of the elements through the cross-section can be assumed, 2D simulations provide almost the same results as 3D simulations and reduce the computational cost substantially.

Finally, all of the simulations have demonstrated that the performance of the structure improves when it is reinforced or retrofitted with fiber reinforced polymers. The degree of improvement depends on the type and configuration of the reinforcement used and on the existing level of damage in the structure when it is applied. In particular case of the RC frame structure, the best CFRP joint reinforcement configuration is to wrap the entire joint by applying the upper, lower and lateral CFRP reinforcements.

Acknowledgements

This work has been supported by CEE-FP6 (LESSLOSS Project, Ref. FP6-50544 (GOCE)), by the Spanish Ministry of Science and Technology (RECOMP Project, Ref. BIA2005-06952 and DECOMAR Project, Ref. MAT2003-08700-C03-02) and by the Spanish Ministry of Public Works (project "Retrofitting and reinforcement of reinforced concrete structures with composite materials. Numerical and experimental developments applied to joint of bars and composites anchorage proposal"). X. Martinez was awarded a fellowship grant by the International Center for Numerical Methods in Engineering (CIMNE), Spain. All support is gratefully acknowledged.

References

[1] Meier U. Strengthening of structures using carbon fibre/epoxy composites. Constr Build Mater 1995;9(6):341–51.
[2] Spadea G, Benicardino F, Swamy R. Structural behaviour of composite RC beams with externally bonded CFRP. J Compos Constr 1998;2(3):132–7.
[3] Khalifa A, Nanni A. Rehabilitation of rectangular simply supported RC beams with shear deficiencies using CFRP composites. Constr Build Mater 2002;16(3):135–46.
[4] Li A, Assih J, Delmas Y. Shear strengthening of RC beams with externally bonded CFRP sheets. J Struct Eng 2001;127(4):374–80.
[5] Li G, Maricherla D, Singh K, Pang S-S, John M. Effect of fiber orientation on the structural behavior of FRP wrapped concrete cylinders. Compos Struct 2006;74(4):475–83.
[6] Khalifa A, Alkhrdaji T, Nanni A, Lansburg S. Anchorage of surface mounted FRP reinforcement. Concr Int: Des Constr 1999;21(10):49–54.
[7] Rabinovitch O, Frostig Y. Nonlinear high-order analysis of cracked RC beams strengthened with FRP strips. J Struct Eng 2001;127(4):381–9.
[8] Barbero EJ. Introduction to composite materials design. Philadelphia, USA: Taylor & Francis; 1999.
[9] Reddy JN. Mechanics of laminated composite plate and shells: theory and analysis. 2nd ed. Boca Raton (FL), USA: CRC Press; 2003.
[10] Sánchez-Palencia E. Homogenization techniques for composite media. Boundary layers and edge effects in composites. Berlin, Germany: Springer-Verlag; 1987. p. 121–92.
[11] Oller S, Miquel J, Zalamea F. Composite material behaviour using a homogenization double scale method. J Eng Mech 2005;131(1):65–79.
[12] Truesdell C, Toupin R. The classical field theories, handbuch der physik iii/i ed.. Berlin, Germany: Springer-Verlag; 1960.
[13] Car E, Oller S, Oñate E. An anisotropic elastoplastic constitutive model for large strain analysis of fiber reinforced composite materials. Comput Methods Appl Mech Eng 2000;185(2–4):245–77.
[14] Rastellini F, Oller S, Salomon O, Oñate E. Advanced serial–parallel mixing theory for composite materials analysis. Continuum basis and finite element applications. In: Oñate E, Owen D, editors. COMPLAS 2003 – Proceeding CD of the VII international conference on computational plasticity; 2003.
[15] Rastellini F, Oller S, Salomon O, Oñate E. Composite materials nonlinear modelling for long fibre reinforced laminates: continuum basis, computational aspects and validations. Comput Struct. doi:10.1016/j.compstruc.2007.04.009.
[16] Salomon O, Rastellini F, Oller S, Oñate E. Fatigue prediction for composite materials and structures. In: Research Technology Organisation (RTO) N, editor. Air Vehicle Technology: AVT-121. Symposium on the evaluation, control and prevention of high cycle fatigue; 2005.
[17] PLCd Manual. Non-linear thermomechanic finite element code oriented to PhD student education, code developed at CIMNE, 1991– to present.
[18] Oller S, Oñate E, Oliver J, Lubliner J. Finite element non-linear analysis of concrete structures using a plastic-damage model. Eng Fract Mech 1990;35(1–3):219–31.
[19] Malvern L. Introduction to the mechanics of a continuous medium. Englewood Cliffs (NJ), USA: Prentice-Hall; 1968.
[20] Lubliner J, Oliver J, Oller S, Oñate E. A plastic-damage model for concrete. Int J Solids Struct 1989;25(3):299–326.
[21] Barbat AH, Oller S, Oñate E, Hanganu A. Viscous damage model for Timoshenko beam structures. Int J Solids Struct 1997;34(30):3953–76.
[22] Mata P, Oller S, Barbat A. Static analysis of beam structures under nonlinear geometric and constitutive behaviour. Comput Methods Appl Mech Eng 2007;196:4458–78.
[23] Mata P, Oller S, Barbat A. Dynamic analysis of beam structures considering geometric and constitutive nonlinearity. Comput Methods Appl Mech Eng 2008;197:857–78.
[24] Oller S, Car E, Lubliner J. Definition of a general implicit orthotropic yield criterion. Comput Methods Appl Mech Eng 2003;192(7–8):895–912.
[25] Car E, Oller S, Oñate E. A large strain plasticity for anisotropic materials–composite material application. Int J Plast 2001;17(11):1437–63.
[26] Benveniste Y, Aboudi J. A continuum model for fibre reinforced materials with debonding. Int J Solids Struct 1984;20(11–12):935–51.
[27] Pulido MDG, Sobrino JA. Los materiales compuestos en el refuerzo de puentes. Rev Int Ingeniería y Estructuras 1998;3(1):75–95.
[28] Gómez Soberón G, Oller S, Barbat A. Evaluación del daño sísmico en puentes de hormigón armado. Rev Int métodos numéricos para el cálculo y diseño en ing 2002;18(2):309–29.
[29] Car E, Zalamea F, Oller S, Miquel J, Oñate E. Numerical simulation of fiber reinforced composites – two procedures. Int J Solids Struct 2002;39(7):1967–86.